POLYMER TESTING

Material properties

Mechanical enhancement of melt-stretched β-nucleated isotactic polypropylene: The role of lamellar branching of β-crystal

CrossMark

Zhongzhu Liu [a], Xianhu Liu [a, b], Guoqiang Zheng [a, *], Kun Dai [a], Chuntai Liu [a, **], Changyu Shen [a], Rui Yin [c], Zhanhu Guo [d]

[a] College of Materials Science and Engineering, The Key Laboratory of Advanced Materials Processing and Mold of Ministry of Education, Zhengzhou University, Zhengzhou, PR China
[b] Institute of Polymer Materials, Friedrich-Alexander University Erlangen-Nuremberg, Martensstrasse 7, 91058 Erlangen, Germany
[c] China Astronauts Research and Training Center, Beijing 100089, China
[d] Integrated Composites Laboratory (ICL), Department of Chemical & Biomolecular Engineering, University of Tennessee, Knoxville, TN 37996, United States

ARTICLE INFO

ABSTRACT

Melt-stretched isotactic polypropylene (iPP) filled with different weight fractions (0, 0.1, 0.2 and 0.4 wt %) of β-nucleating agent (β-NA) was extruded via a single screw extruder with a slit die and immediately melt-stretched at the die exit. The microstructure and mechanical properties (i.e., monotonic tensile, step-cycle and stress relaxation behavior) of these samples were analyzed. Unexpectedly, the lamellar branching of β-crystal, which is similar to lamellar branching of α-crystal, is observed in melt-stretched β-nucleated iPP. More interestingly, it is found that, compared with other samples, iPP containing 0.2 wt % of β-NA has the best mechanical properties. Through thorough analysis of various structural characterizations, the improved tensile strength obtained from step-cycle tests and viscous force obtained from stress relaxation measurements for iPP with 0.2 wt% of β-NA is ascribed to lamellar branching of β-crystal. The study is an example of preparing high performance polymers via practical polymer processing methods.

© 2017 Published by Elsevier Ltd.

1. Introduction

Isotactic polypropylene (iPP) is one of the most important commercial polymers owing to its low manufacturing cost and versatile properties. Moreover, it is a typical polymorphic plastic with at least four crystal modifications, namely, namely, α, β, γ and mesomorphic smectic [1,2]. Among them, β-crystal shows excellent toughness and ductility, so it has received considerable attention for academic interests and industrial applications [3–6]. However, β-crystal can be only generated under some special conditions, such as quenching [3], abrupt temperature gradient [4], shearing or elongation deformation [5,6] as well as the addition of β-nucleating agent (β-NA) [7]. Among these methods, the addition of β-NA is the most effective and accessible method to obtain high β-crystal content in iPP [7,8].

Processing strongly affects the microstructure of semi-crystalline polymer products. During practical polymer processing, such as injection molding and extrusion, intense shear or stretching flow is inevitably involved. Widely accepted conclusions are that flow field can significantly influence the crystalline morphology and final properties [9,10]. Hence, flow-induced crystallization is considered to be a pathway to fabricate high performance polymer products. Unlike shear, stretching is much more effective in inducing chain extension [11].

For semi-crystalline polymer, various structural transformations, e.g., reorientation, fragmentation and recrystallization occur during uniaxial tensile deformation [12–14]. Such structural transformations were mainly observed at large strains, hence this deformation domain has received considerable attention. However, certain alterations of polymer structure were also observed in the early stages of drawing below the yield point (i.e., elastic region) [15–18]. The loading-unloading behavior of polypropylene (PP) and low density polyethylene (LDPE) below the yield point was investigated [15], and a remarkable decrease in residual strains in comparison with those predicted by conventional viscoelastic models was found. Additionally, study of the influence of unloading

rate on stress-strain behavior of high density polyethylene (HDPE) below yield point was carried out [18]. It was found that the residual strain decreased with decreasing unloading rate. Moreover, mechanical behavior of HDPE subjected to uniaxial cyclic loading-unloading below the yield point was investigated by Hizoum [17]. It was concluded that small-strain cyclic uniaxial loading-unloading of HDPE at constant strain rate leads to accumulation of nanovoids in the material. The volume fraction of these nanovoids tends to saturate with number of cycles. Tscharnuter et al. [16] also reported the cavitation of isotactic polypropylene (iPP) caused by uniaxial tensile deformation in the pre-yield regime. It has been found that stress whitening is related to the amount of cavitation. In the aforementioned literature, researchers concentrated mainly on the cyclic deformation behavior of pure polyethylene or iPP below the yield point. However, to the best of our knowledge, studies on microstructure determined step-cycles and stress relaxation behavior of β-nucleated iPP below yield point are relatively rare. In particular, there are no studies investigating the influence of crystalline morphology of β-crystal (i.e., lamellar branching) on the mechanical properties. The main problem might be that, with the introduction of β-NA, polymorphic composition and crystallinity of iPP matrix are altered simultaneously, with the change of crystalline morphology in most cases. Therefore, it is difficult to estimate the individual effect of crystalline morphology among various influential factors.

In this study, lamellar branching structure of β-crystal in melt-stretched β-nucleated iPP was obtained, and the influence of this lamellar branching structure of β-crystal on mechanical properties was investigated in detail. It is very interesting to find that the enhancement of mechanical properties can be mainly attributed to the improved connection between inter-crystallites through the formation of different β-crystal morphology. The findings of this study are useful for preparing high performance polymers through practical processing methods.

2. Experimental section

2.1. Materials

Commercial iPP (T30S) with a melt flow index of 2.6 g/10min (190 °C, 21.6 N) and a mass average molar mass of ca. 1.1×10^5 g/mol was bought from Lanzhou Petroleum Chemical Co., China. The rare earth β-NA (WBG-II), was kindly supplied by Guangdong Winner Functional Materials Co., Ltd. Detailed information about it has been presented in our previous work [19,20] and Fig. S1.

2.2. Sample preparation

The iPP granules and β-NA powders were first melt mixed in a twin-screw extruder (Giant, SHJ-20B). The temperature profile from hopper to die was 150, 160, 170, 185, 195 and 190 °C. After pelletizing and drying, the mixture was extruded through a single screw extruder (Haake Polylab System-Rheomex 252p series) with a slit die (1 mm × 50 mm). The temperature profile from hopper to die of extruder was 165, 180, 195 and 185 °C. In order to reduce the shear stress in the die as much as possible, the screw rotating speed was set at 0.6 rpm. Accordingly, the melt flow rate in the die was extremely low (about 0.9 cm/min) and the effect of shear stress can, therefore, be neglected. Once iPP melt left the die, it was uniaxial-stretched at a fixed rate of 30 cm/min. The thickness of melt-stretched iPP was ca. 65 μm. All the take-up rollers were kept at room temperature. A schematic illustration of extrusion-stretching set-up and a representative photograph of melt-stretched iPP are shown in Fig. S2a and b. For convenience, the melt-stretched iPP were labeled as iPP-X, herein "X" represents β-NA content.

2.3. Characterization

2.3.1. Tensile test

The mechanical experiments were carried out according to ISO 527-3. The tensile test was performed using a universal tensile testing machine (UTM2203, Shenzhen Suns Technology Stock Co., Ltd, China) with a 100 N load cell at room temperature. The crosshead speed for monotonic tensile tests was 1 mm/min. For step-cycle tests, the crosshead speed was 1 mm/min (corresponding strain rate 0.001 s^{-1}) with an initial grip separation of 16 mm. Step-cycle tests were carried out according to the following procedure: (a) specimens were stretched up to a designed strain, i.e., $\varepsilon = 5\%$; (b) unloaded down to the minimum stress, i.e., $\sigma = 0$; (c) reloaded up to $\varepsilon = 5\%$; (d) unloaded down to $\sigma = 0$; (e) …. etc. Each test involved $n = 10$ cycles of loading-unloading. For stress relaxation measurements, the sample was stretched first to a fixed strain (i.e., 5%) at a constant crosshead speed of 1 mm/min. Subsequently, the strain was held constant and relaxation process was recorded. The relaxation time was set as 30 000 s.

All specimens were cut from the center of melt-stretched iPP along uniaxial-stretching direction using a dumbbell-shaped die. A photograph showing the typical appearance of specimens is presented in Fig. S2d. The tensile deformation direction was along the uniaxial-stretching direction. The reported values were calculated as the average of over five specimens.

2.3.2. Two-dimensional wide-angle X-ray diffraction (2D-WAXD) and small-angle X-ray scattering (-SAXS)

Two-dimensional wide-angle X-ray diffraction (2D-WAXD) and small-angle X-ray scattering (-SAXS) experiments were performed at the beamline BL16B1 of Shanghai Synchrotron Radition Facility (SSRF). The X-ray wavelength was 0.124 nm. A MAR 165 CCD detector (2048 × 2048 pixels with pixel size 80 μm) was employed to collect 2D-WAXD and -SAXS patterns, which was placed 178 mm and 5200 mm away from the samples, respectively.

In order to get the maximum diffraction intensity, several melt-stretched iPP were stacked with a total thickness of about 1 mm. All samples were arranged along the melt-stretching direction. The region selected for characterization is schematically shown in Fig. S2c.

2.3.3. Differential scanning calorimetry (DSC)

Thermal analysis was carried out in a TA DSC-2920 differential scanning calorimeter under nitrogen atmosphere. The weight of specimen was about 6 mg. The specimens were heated from room temperature to 200 °C at a rate of 10 °C/min and kept for 5 min to eliminate the heat history then cooled to 40 °C at the same rate.

2.3.4. Scanning electron microscopy (SEM)

Crystalline morphology of melt-stretched iPP was investigated using a field emission scanning electron microscope FESEM (JEOL JSM-7500F, Japan). Before SEM observation, the specimens were etched by a solution mixture of 1:1 volume of concentrated sulfuric acid and nitric acid by solving 0.7 wt % of potassium permanganate, and the etched surface was sputter-coated with a layer of gold.

3. Results and discussion

3.1. Structural orientation of melt-stretched samples

Fig. 1 shows the 2D-WAXD and 2D-SAXS patterns of melt-stretched iPP. From 2D-WAXD patterns, apparent arc-like diffractions in the meridional direction are seen for all samples, which is indicative of obvious molecular orientation [21,22]. In 2D-SAXS patterns, a two-spot pattern in the equatorial direction is clearly
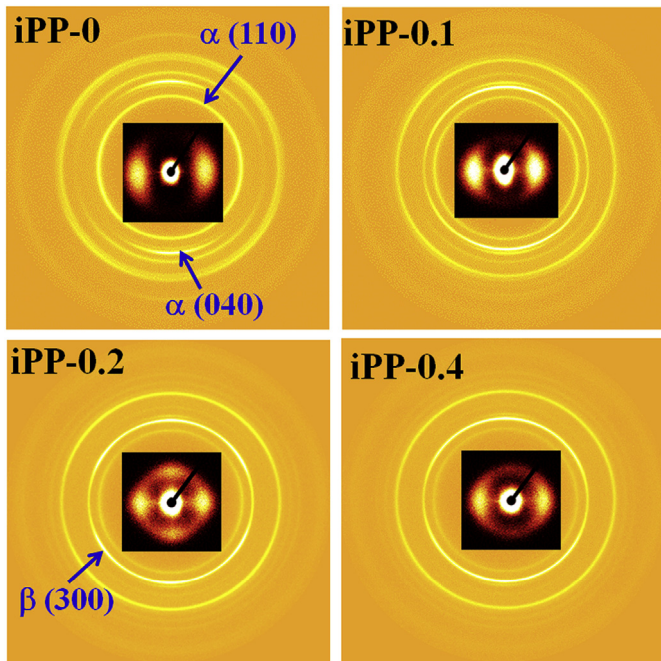
Fig. 1. 2D-WAXD patterns of melt-stretched iPP. The insets show the corresponding 2D-SAXS pattern. The melt-stretched direction is horizontal.

observed, which indicates the existence of stacks of oriented crystalline lamellae [22]. Therefore, it can be concluded that significant molecular and lamellar orientation appear in melt-stretched iPP. To further evaluate the orientation level of these samples, the orientation parameter was calculated using Herman's orientation parameter (f). Detailed calculated process is in supplementary material and the calculated orientation parameters of samples are listed in Table 1. As shown in Table 1, f_{WAXD} and f_{SAXS} increase significantly until β-NA content reaches 0.2 wt % and then there is no apparent difference as β-NA content further increased, which can be understood as follows: as indicated by DSC results, onset and peak crystallization temperatures increases sharply with increasing β-NA content from 0 to 0.2 wt %, which must lead to hinder relaxation of oriented iPP chains [23].

More interestingly, from 2D-WAXD patterns, it can be seen that six arc-like diffractions located in the meridional direction and far from the meridional direction of β(300) for iPP-0.2. This is regarded as an indication of parent-daughter lamellar branching through homoepitaxy between β-crystal themselves [20,24—27]. Moreover, with respect to 2D-SAXS patterns for iPP-0.2, except for two distinct scattering maxima along the equatorial direction, two scattering maxima along meridional direction were found. It is generally accepted that equatorial maxima in 2D-SAXS patterns can be attributed to the formation of parent lamellae structure, while the meridional maxima could be responsible for the stacks of daughter lamellae [28]. Therefore, above results indicate that lamellar

branching structure is formed in iPP-0.2.

In order to gain more insight into the changes of parent-daughter lamellar branching, azimuthal scans of β(300) and α(110) were obtained from 2D-WAXD patterns, as presented in Fig. 2. Obviously, except for iPP-0, α(110) intensity curves show six-peaks, which is indicative of a mixed bimodal orientation for α-crystal. That is, lamellar branching structure is found in α-crystal for β-nucleated samples. Additionally, six diffraction peaks for β(300) intensity curve were found in β-nucleated samples, which may be indicative of lamellar branching structure in β-crystal [20,24—27]. Moreover, with increasing β-NA, the relative intensity of the reflection from daughter lamellae with respect to that of parent lamellae is apt to rise first and then decrease. To obtain more quantitative information about this characteristic, the fractions of daughter lamellae (R) and parent-daughter ratio ($[R]$) for α-crystal and β-crystal were estimated according to Eqs. S3 and S4 in supplementary material [29,30]. Because the lamellar branching of α-crystal has been investigated in our previous works [20,26], it will not be discussed further here. As listed in Table 1, it is clear that R_β rises first and then decreases with increasing β-NA content, while the reverse trend is found for $[R]_\beta$. This can be understood as follows: On the one hand, this is attributed to the effective nucleating ability of β-NA. For iPP-0.1, β-NA has good dispersion for relatively low levels, thus, bundle-like β-spherulites are formed. On the other hand, β-NA substances can easily recombine into needle-like nucleus during flow and orient along the flow direction [10,31]. Therefore, the excessive β-NA leads to confined space between needle-like nucleuses. The lamellae growing perpendicular to the surface of β-NA (especially for the needle-like nuclei) have been observed [31,32]. Thus, the confined space is unfavorable for the formation of lamellar branching structure of β-crystal [20]. In other words, "daughter lamellae" of β-crystal are prevented in iPP-0.4. By contrast, the obvious lamellar branching of β-crystal is formed in iPP-0.2, which is ascribed to the fact that the β-NA content is optimal and there is sufficient space for lamellar branching structure of β-crystal.

3.2. Crystalline structure of melt-stretched samples

To obtain more insight into crystallization behavior, one-dimensional (1D) WAXD curves are obtained from 2D-WAXD patterns and illustrated in Fig. 3a. Crystallinity parameters are estimated using the method in supplementary material. As shown in Fig. 3b, a slightly increase in X_c with continuously increasing β-NA content from 0 to 0.2 wt % is observed. However, X_β increases remarkably when β-NA content increases from 0 to 0.2 wt %. These results show that the introduction of β-NA, not only induces the generation of β-crystal, but also slightly increases X_c. However, X_c and X_β experience no substantial increase with further increasing β-NA content. This can be ascribed to the fact that β-NA content reaches its saturation point, i.e., 0.2 wt %. Therefore, too much β-NA has no apparent effect on inducing the formation of β-crystal [33]. Moreover, $X_{\beta-D}$ for iPP-0.2 is larger than that of iPP-0.1 and iPP-0.4, which has been discussed above. As listed in Table 2, the crystalline sizes decrease with increase of β-NA content. This is ascribed to more primary nuclei and shish structures in a confined space induced by addition of β-NA [26]. Therefore, the growth of lamellae tends to be inhibited, resulting in smaller crystallite size.

Fig. 4 shows one-dimensional correlation function $K(z)$ for the lamellar stacks obtained from 2D-SAXS patterns. According to the $K(z)$ curves, L, L_a and L_c can be obtained [34], and calculated results are listed in Table 2. It has been well established that L of β-crystal is generally larger than that of α-crystal [10,26,35]. Thus, it is understandable that the increase of L in β-nucleated samples can be ascribed to the formation of high content of β-crystal. Moreover, in

Table 1
f_{WAXD}, f_{SAXS}, R_β, R_α, $[R]_\beta$ and $[R]_\alpha$ of melt-stretched iPP.

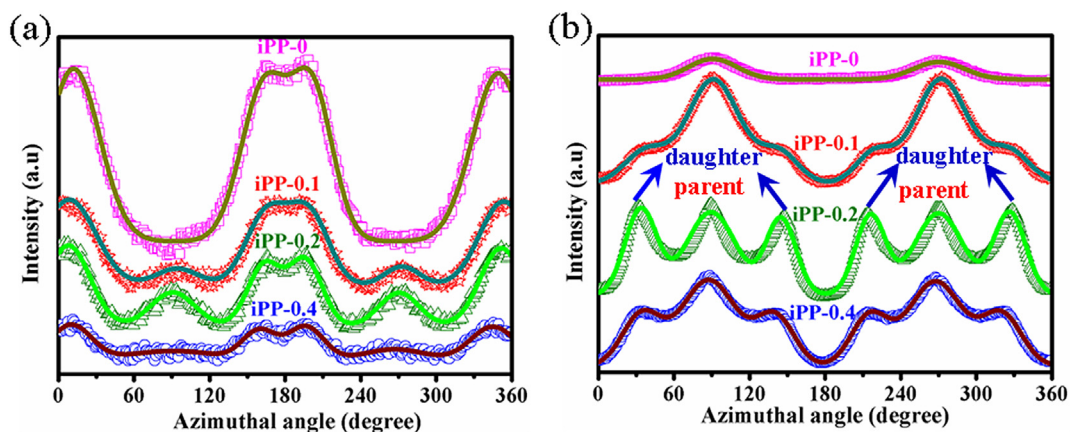| sample	iPP-0	iPP-0.1	iPP-0.2	iPP-0.4
f_{WAXD}	0.62	0.69	0.85	0.80
f_{SAXS}	0.53	0.59	0.86	0.84
R_β	–	0.30	0.55	0.39
$[R]_\beta$	–	2.33	0.85	1.57
R_α	–	0.88	0.74	0.72
$[R]_\alpha$	–	0.13	0.34	0.40

Fig. 2. Azimuthal intensity curves of α(110) plane (a) and β(300) plane (b) of melt-stretched iPP.
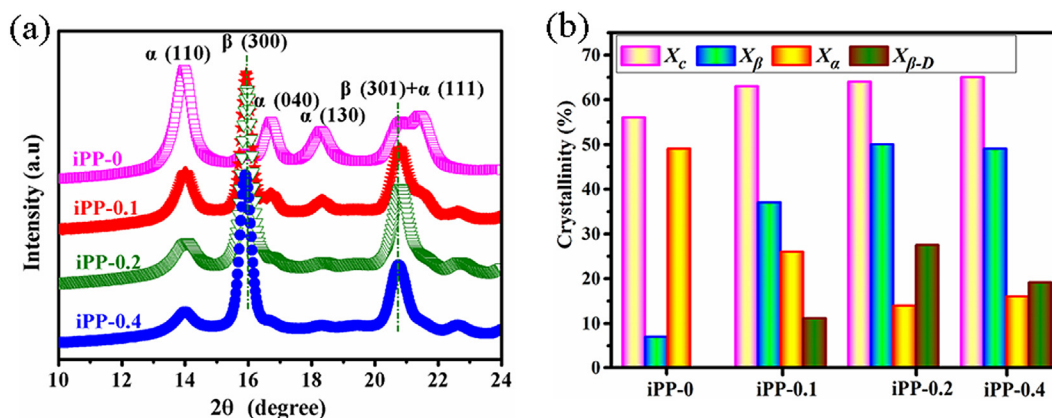

Fig. 3. 1D-WAXD curves (a) and calculated crystallinity (b) of melt-stretched iPP.

Table 2
Crystal microstructure parameters of melt-stretched iPP.

sample	L(nm)	L_a(nm)	L_c(nm)	L_{110}(nm)	L_{040}(nm)	L_{300}(nm)
iPP-0	10.38	4.52	5.86	9.92	14.99	21.97
iPP-0.1	12.83	5.51	7.32	9.77	13.58	16.07
iPP-0.2	13.49	6.01	7.48	8.84	13.07	16.18
iPP-0.4	13.72	6.12	7.60	8.39	12.20	15.61

our case, crystallization is speeded up after addition of β-NA (this can be proved by the DSC results), providing a relatively longer effective time for crystallization, thus, more perfect and thicker crystals are formed. Therefore, it is reasonable that L_c gradually increases.

3.3. Thermal and crystallization analysis of melt-stretched samples

The melting curves for all melt-stretched iPP are shown in Fig. 5a. Clearly, there is a dominant peak around 167 °C, which is attributed to the melting of α-crystal. In addition, two additional melting peaks appear at around 144 °C and 150 °C. In our case, the peak located at 144 °C can be associated with the melting of initial β-crystal, whereas endotherm located at 150 °C is related to the melting of perfected or thickened lamellae, which is formed upon heating by partial melting and recrystallization of initially formed β-crystals [36]. Interestingly, it is obvious that the peak located at 144 °C becomes stronger with increasing β-NA content, indicating
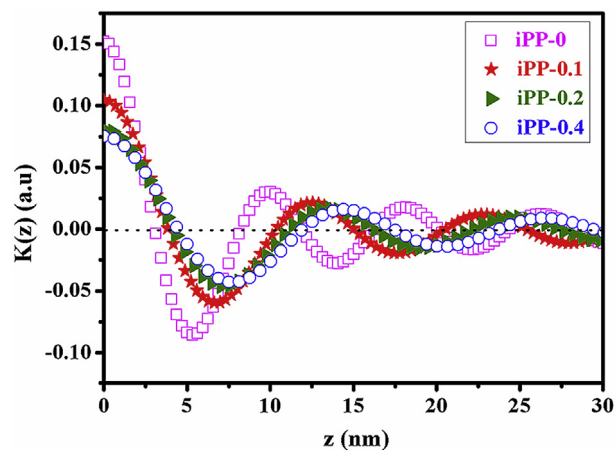

Fig. 4. One dimensional correlation function $K(z)$ obtained from 1D-SAXS curves of melt-stretched iPP.

that β-NA can effectively induce the formation of β-crystal. Meanwhile, the overall crystallinity (X_{c-DSC}) and relative content of β-crystal ($K_{β-DSC}$) are also evaluated from DSC melting curves according to Eqs. S12 and S13 [37] in supplementary material, which are presented in Fig. 5b. It is seen that $K_{β-DSC}$ rapidly increase until β-NA content reaches a critical value of 0.2 wt % and then it keeps almost constant. It should be noted that there is some discrepancy

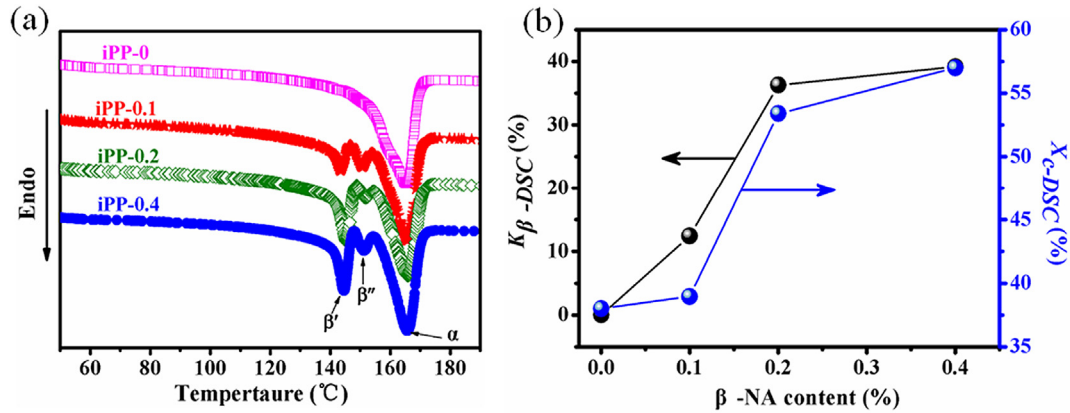**Fig. 5.** The DSC melting curves (a) and the overall crystallinity (X_{C-DSC}) and relative content of β-crystal ($K_{\beta-DCS}$) (b) of melt-stretched iPP.

between the results assessed by DSC and those estimated by 2D-WAXD, as mentioned above. Such divergence can be explained as follows: some unstable β-crystal with thinner crystalline lamellas are transformed to α-crystal during DSC heating program, which has been reported in other work [38]. In addition, since 2D-WAXD is performed under room temperature, the β-α phase transformation can be excluded. However, this variation tendency of $K_{\beta-DSC}$ is inconsistent with the 2D-WAXD results. Moreover, as shown in Fig. 5b, X_{c-DSC} gradually increases with the increase of β-NA content. However, the crystallinity obtained by 2D-WAXD is considerably larger than that of obtained by DSC method. This is attributed to the contribution of crystalline-amorphous transition layers or dense rigid amorphous phase existing in between lamellar crystal grains during 2D-WAXD experiments [39].

The nonisothermal crystallization curves obtained after removing thermal and mechanical history of samples are presented in Fig. 6a. The evident change in these exothermic curves suggests that β-NA substantially influences nonisothermal crystallization behavior of samples. On the basis of these curves, detailed crystallization parameters, including onset crystallization temperature (T_{onset}) and peak crystallization temperature (T_p), can be obtained, as presented in Fig. 6b. It can be clearly seen that the addition of β-NA has significantly improved T_{onset} and T_p [40]. For iPP-0, appeared to be at about 113.9 °C, whereas this value rapidly increased to 126.2 °C for iPP-0.2. These results confirm the effective nucleating ability of β-NA. However, such effect was not linearly dependent on β-NA content. Compared with iPP-0.2, T_p of iPP-0.4 (i.e., 126.0 °C) keeps almost constant. In other words, the saturation point of β-NA

in our case is 0.2 wt %. The results agree well with the calculated crystallinity from 2D-WAXD results. On the other hand, higher T_{onset} is indicative of a substantial decrease in supercooling ($\Delta T = T_m^0 - T_p$, where T_m^0 is the equilibrium melting temperature, T_p is the crystallisation temperature) needed to initiate the crystallization process, providing a relatively longer effective time for crystallization, thus, perfect crystals are formed [41]. Moreover, L_c can be associated with ΔT, i.e., $L_c = k \frac{1}{\Delta T}$, where k is a constant [42]. This is in good agreement with the increase of L_c in Table 2.

3.4. Morphology observation of melt-stretched samples

Based on the above results, it is concluded that β-crystal content and microstructure parameters are very similar in iPP-0.2 and iPP-0.4. However, obvious lamellar branching structures are formed in iPP-0.2, which is evidently different from that of iPP-0.4. Therefore, the comparison of crystalline morphology between iPP-0.2 and iPP-0.4 is presented in Fig. 7. It can be clearly seen in Fig. 7a and a' that there are three types of β-crystal morphology, namely, β-cylindrulite (see blue rectangle), fan-shape β-crystal (see green arrows) and bundle-like β-crystal (see pink ellipse). The different crystalline morphologies can lead to the formation of reticular crystalline structure in iPP-0.2. With respect to iPP-0.4 in Fig. 7b and b', the morphology of β-crystal is evidently different from that of iPP-0.2. Most of the field of view is occupied by horizontal β-crystal lamella, as indicated by the blue arrows. The possible reason for the different morphology can be interpreted as follows: under the same processing conditions, because of relatively low content of β-NA in
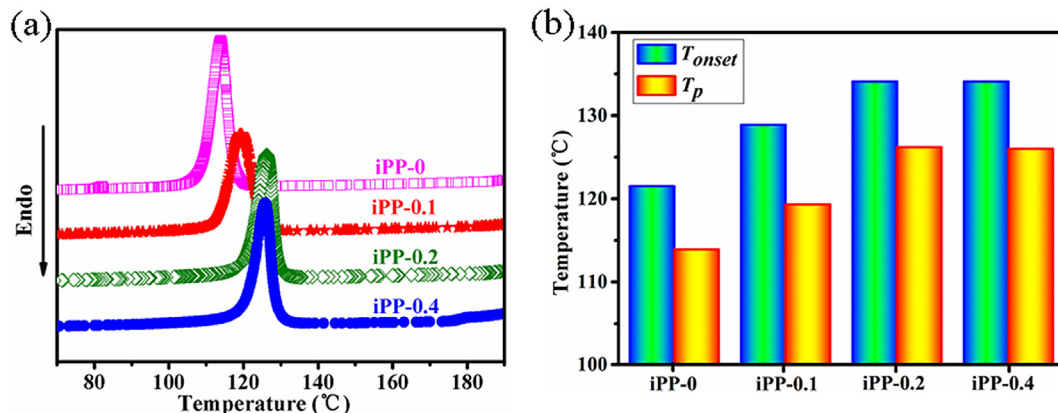

Fig. 6. Nonisothermal crystallization curves (a) and crystallization parameters (T_{onset} and T_p) (b) of melt-stretched iPP.
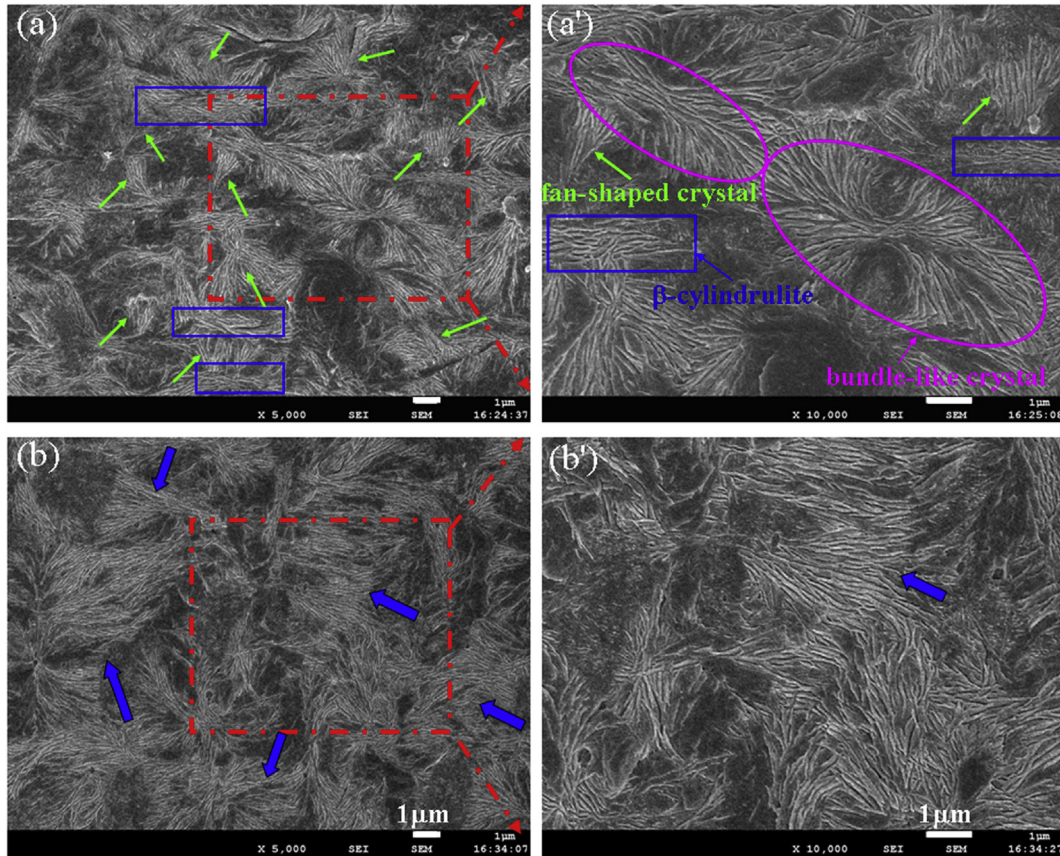
Fig. 7. SEM micrographs of iPP-0.2 (a and a') and iPP-0.4 (b and b'); (a') is the magnification of (a); (b') is the magnification of (b). The melt-stretched direction is horizontal.

iPP-0.2, there is sufficient space for β-crystal induced by β-NA to grow. By contrast, in iPP-0.4, because of the excessive β-NA content (conformed by the aforementioned 2D-WAXD and DSC results), there is less space for β-crystal to grow. Therefore, the β-crystal induced by β-NA was restrained spatially, leading to growth of β-crystal along the horizontal direction. Since different crystalline morphologies have been generated in samples, we are very curious whether such different crystalline morphologies can lead to the better mechanical properties. Thus, in the following sections, the relationship between mechanical properties and microstructure is explored.

3.5. Mechanical properties of melt-stretched samples

The stress-strain curves are depicted in Fig. 8a, and the inset picture illustrates the small deformations zone. It is seen that the addition of β-NA into iPP matrix has a significant influence on tensile deformation behavior. In order to quantitatively estimate tensile properties, the average values of ultimate tensile strength and toughness were determined from the stress-strain curves and summarized in Fig. 8b. W_b, the total mechanical energy per unit volume consumed by the sample when straining it to break is usually used as a measure for the toughness of a material [43]. W_b can be obtained by integrating the area under the stress-strain
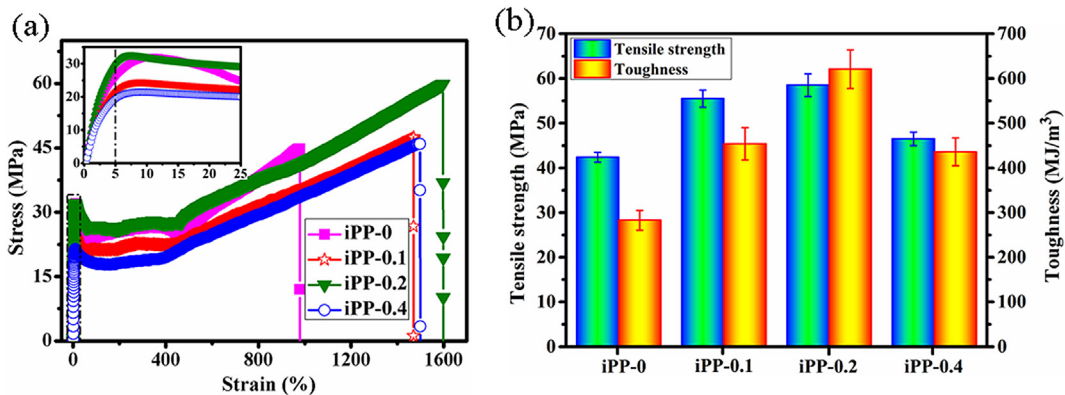

Fig. 8. Stress-strain curves (a) and tensile properties (tensile strength and toughness) (b) of melt-stretched iPP. Inset picture are the enlarged one at small deformations of selected section.
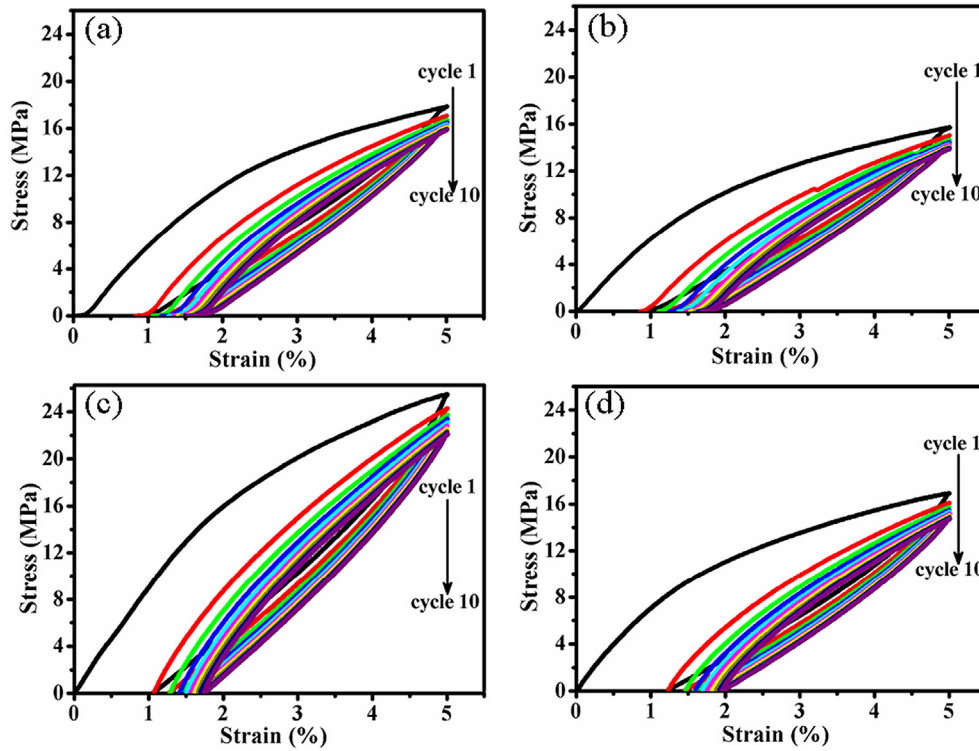
Fig. 9. Step-cycle test curves with a constant strain of 5% for iPP-0 (a); iPP-0.1 (b); iPP-0.2 (c); iPP-0.4 (d).

curves by the following equation [43]: $W_b = \int_0^\varepsilon \sigma d\varepsilon$. As shown in Fig. 8b, unexpectedly, the iPP-0.2 exhibits maximum tensile strength and toughness. Based on the comprehensive analysis of aforementioned microstructure, one may naturally deduce that such simultaneous enhancement of strength and toughness of iPP-0.2 probably depends on the different crystalline morphology of β-crystal.

In addition, from the monotonic stress-strain curves in Fig. 8a, it can be clearly observed that all the samples exhibit a yield point at strain *ca.* 6%, which represents the onset of permanent damage. Beyond the yield point, the samples present a region of cold drawing at almost constant stress (i.e. plastic flow region). Subsequently, significant strain hardening occurred followed by rupture. It is well known that semi-crystalline polymers follow Hooke's law before yield point and exhibit instantaneous elastic deformation,

Fig. 10. Maximum tensile strength of samples at each cycle.

which is believed to be due to the stretching of the short tie chains in the amorphous phase [17]. To further reveal the effect of microstructure on the elastic deformation behavior of samples, step-cycle and stress relaxation experiments were investigated for melt-stretched iPP in the strain range of below 5% (i.e., below yield point).

Fig. 9 presents the results of step-cycle tests for samples conducted with a constant strain of 5%. The loading-unloading curves gradually exhibit overlapping after the 8th cycle, indicating that the molecular arrangement in amorphous phase would become stable from 8th to 10th cycles. In order to clearly understand this behavior, the maximum tensile strength of samples at each cycle was determined, as shown in Fig. 10. It is easily seen that maximum tensile strength decreases with increasing cycles. However, with further increase of cycles, the decrease is negligable, indicating that a stable molecular arrangement is formed in the amorphous phase. Stretching of a semi-crystalline polymer material can be viewed as stretching of two interpenetrated networks built up by interlocked lamellae (the crystalline phase) and entangled amorphous phase [44]. The macromolecular chains which exist in both crystalline and amorphous regions will form tie molecules connecting crystals and amorphous region, acting as physical cross-links [45]. During deformation, the deformation of tie molecules from "relatively oriented" to extended chains. Moreover, the deformation of tie molecules is considered as the vital factor determining mechanical strength of samples when being drawn [46,47]. Therefore, during the 1st cycle loading, the amorphous chains can be stretched into relatively extended-chains. During the following unloading, the extended chains have not enough time to relax at shorter time scale, i.e., the interval between 1st cyle and 2nd cycle, and then subject to loading again immediately (i.e., 2nd cycle). Thus, during the 2nd cycle, each entangled chain is less strong than in the 1st cycle. In light of this, it is reasonable that the stress which forces entangled amorphous phase to extend becomes smaller. Therefore,
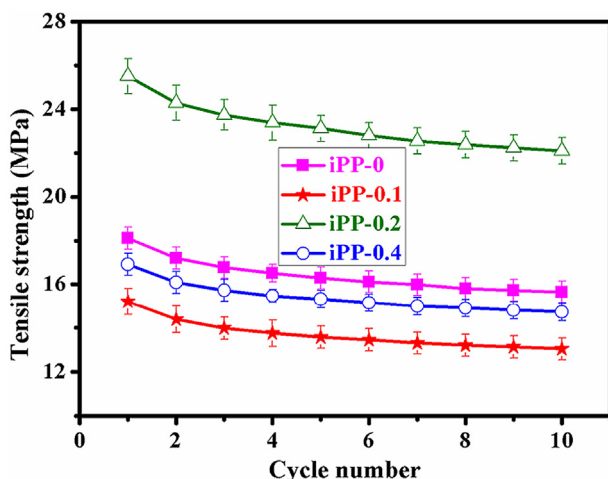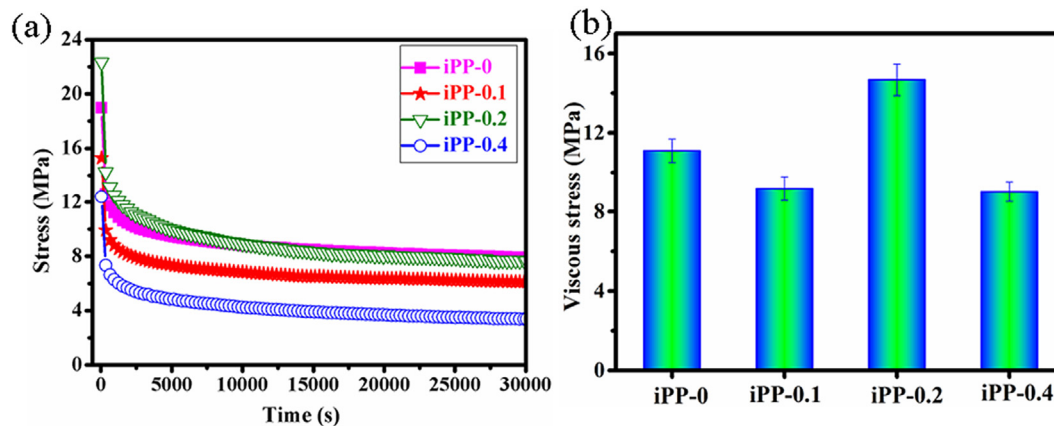
Fig. 11. The stress relaxation curves of melt-stretched iPP with a fixed strain of 5% (a) and the viscous forces of samples after a relaxation time of 30000 s (b).

with further increasing cycles, the tensile strength gradually decreases. Finally, the stress-strain curves followed the same tendency for 9th and 10th cycles, suggesting that the relatively stable extended molecular arrangement in amorphous phase is formed.

On the other hand, as shown in Fig. 10, tensile strength of iPP-0.2 is obviously higher than that of other samples, which is attributed to the lamellar branching structure of β-crystal. This is in consistent with the tensile properties shown in Fig. 8b. The lamellar branching can interconnect neighboring lamellae. It is expected that the presence of lamellar branching structures can enhance the inter-lamellar coupling [14]. The enhanced inter-lamellar coupling results in higher resistance to deformation, i.e., a higher tensile strength. Additionally, according to Fig. 7, three types of β-crystal morphology are generated in iPP-0.2. The connection between β-crystal can be improved due to such different crystalline morphologies, i.e., reticular connected β-crystal is formed in iPP-0.2. Therefore, during deformation, the reticular crystalline system possesses good integrity for resisting deformation, indicating the enhanced tensile strength for iPP-0.2.

Fig. 11a shows typical examples of stress relaxation curves for each sample. Stress (σ_0) decreased sharply and eventually decayed to a final plateau value, σ_t. Therefore, the viscous stress ($\Delta\sigma$) of samples can be calculated by $\Delta\sigma = \sigma_0 - \sigma_t$ [14,48], and the results are shown Fig. 11b. It is found that iPP-0.2 shows the maximum value of $\Delta\sigma$. The variation tendency is similar with that of tensile strength for each cycle. It has been reported that the smaller L_{hkl}, the better resistance to stress relaxation (i.e., higher $\sigma_t\sigma_t$) [45]. As shown in Table 2, L_{hkl} gradually decreases with increasing β-NA content. Therefore, compared to iPP-0, σ_t of melt-stretched β-nucleated iPP increases. Moreover, σ_0 is related to crystalline form and morphology [14,49]. From the 2D-WAXD and DSC results, it is seen that the α-crystal content is extremely high in iPP-0, thus leading to higher σ_0. Therefore, the viscous stress of iPP-0 is higher than that of iPP-0.1 and iPP-0.4. However, the viscous stress of iPP-0.2 is higher than that of other samples. This is associating with the obvious lamellar branching structure of β-crystal in iPP-0.2, leading to enhanced inter-lamellar coupling. The enhanced inter-lamellar coupling will result in higher viscous force.

4. Conclusions

iPP filled with different weight fractions of β-NA was extruded via a slit die and immediately melt-stretched at the die exit. Subsequently, effects of β-NA content on microstructure and mechanical properties of melt-stretched β-nucleated iPP were investigated. Unexpectedly, the obvious lamellar branching of β-crystal, which is

similar to the lamellar branching of α-crystal, is observed in iPP-0.2. Moreover, monotonic tensile tests indicate that simultaneous enhancement of strength and toughness has been successfully realized in iPP-0.2, which is ascribed to the different β-crystal morphology induced by β-NA. In addition, the tensile strength obtained from step-cycle tests and viscous force obtained from stress relaxation measurements of iPP-0.2 is higher than that of other samples. Through thorough analysis of various structural characterizations, the improvement of tensile strength and viscous force of iPP-0.2 is attributed to the reticular β-crystal structure formed by different β-crystal morphology.

Acknowledgments

Appendix A. Supplementary data

Supplementary data related to this article can be found at http://dx.doi.org/10.1016/j.polymertesting.2017.01.002.

References

[1] B. Lotz, S. Graff, C. Straupe, J. Wittmann, Single crystals of γ phase isotactic polypropylene: combined diffraction and morphological support for a structure with non-parallel chains, Polymer 32 (1991) 2902—2910.
[2] S.W. Wang, W. Yang, Y.J. Xu, B.H. Xie, M.B. Yang, X.F. Peng, Crystalline morphology of β-nucleated controlled-rheology polypropylene, Polym. Test. 27 (2008) 638—644.
[3] A. Turner-Jones, Crystallinity in isotactic polyolefins with unbranched side chains, Die Makromol. Chem. 71 (1964) 1—32.
[4] Y. Fujiwara, Double-melting behavior of beta phase of isotactic polypropylene, Colloid. Polym. Sci. 253 (1975) 273—282.
[5] D. Byelov, P. Panine, K. Remerie, E. Biemond, G.C. Alfonso, W.H. de Jeu, Crystallization under shear in isotactic polypropylene containing nucleators, Polymer 49 (2008) 3076—3083.
[6] J. Varga, J. Karger-Kocsis, Interfacial morphologies in carbon fibre-reinforced polypropylene microcomposites, Polymer 36 (1995) 4877—4881.
[7] J. Varga, A. Menyhard, Effect of solubility and nucleating duality of N, N'-dicyclohexyl-2, 6-naphthalenedicarboxamide on the supermolecular structure of isotactic polypropylene, Macromolecules 40 (2007) 2422—2431.
[8] Y.D. Lv, Y.J. Huang, M.Q. Kong, G.X. Li, Improved thermal oxidation stability of polypropylene films in the presence of β-nucleating agent, Polym. Test. 32 (2013) 179—186.
[9] F. Luo, C. Geng, K. Wang, H. Deng, F. Chen, Q. Fu, B. Na, New understanding in tuning toughness of β-polypropylene: the role of β-nucleated crystalline morphology, Macromolecules 42 (2009) 9325—9331.
[10] Q. Sheng, Y. Zhang, C. Xia, D. Mi, X. Xu, T. Wang, J. Zhang, A new insight into the effect of β modification on the mechanical properties of iPP: the role of

crystalline morphology, Mat. Des. 95 (2016) 247—255.

[11] F.M. Abuzaina, B.D. Fitz, S. Andjelić, D.D. Jamiolkowski, Time resolved study of shear-induced crystallization of poly (p-dioxanone) polymers under low-shear, nucleation-enhancing shear conditions by small angle light scattering and optical microscopy, Polymer 43 (2002) 4699—4708.

[12] R. Hiss, S. Hobeika, C. Lynn, G. Strobl, Network stretching, slip processes, and fragmentation of crystallites during uniaxial drawing of polyethylene and related copolymers. A comparative study, Macromolecules 32 (1999) 4390—4403.

[13] Q. Fu, Y.F. Men, G. Strobl, A molar mass induced transition in the yielding properties of linear polyethylene, Polymer 44 (2003) 1941—1947.

[14] B. Na, Q. Zhang, Q. Fu, Y.F. Men, K. Hong, G. Strobl, Viscous-force-dominated tensile deformation behavior of oriented polyethylene, Macromolecules 39 (2006) 2584—2591.

[15] V. Oshmyan, S. Patlazhan, Y. Remond, Simulation of small-strain deformations of semi-crystalline polymer: coupling of structural transformations with stress-strain response, J. Mat. Sci. 39 (2004) 3577—3586.

[16] D. Tscharnuter, M. Jerabek, Z. Major, G. Pinter, Irreversible deformation of isotactic polypropylene in the pre-yield regime, Eur. Polym. J. 47 (2011) 989—996.

[17] K. Hizoum, Y. Rémond, S.A. Patlazhan, Coupling of nanocavitation with cyclic deformation behavior of high-density polyethylene below the yield point, J. Eng. Mat. Technol. 133 (2011) 1—5.

[18] S.A. Patlazhan, K. Hizoum, Y. Rémond, Stress-strain behavior of high-density polyethylene below the yield point: effect of unloading rate, Polym. Sci. Ser.A 50 (2008) 507—513.

[19] Z.Z. Liu, G.Q. Zheng, K. Dai, C.T. Liu, C.Y. Shen, Simultaneously improving tensile strength and toughness of melt-spun β-nucleated isotactic poly-propylene fibers, J. Appl. Polym. Sci. 133 (2016) 43454.

[20] Z.Z. Liu, X.H. Liu, G.Q. Zheng, K. Dai, C.T. Liu, C.Y. Shen, New insight into lamellar branching of β-nucleated isotactic polypropylene upon melt-stretching: WAXDd and SAXS study, J. Mat. Sci. 50 (2015) 599—604.

[21] Z. Ping, W. Ke, Y. Hong, Z. Qin, R.N. Du, F. Qiang, Excellent tensile ductility in highly oriented injection-molded bars of polypropylene/carbon nanotubes composites, Polymer 48 (2007) 5688—5695.

[22] P.W. Zhu, G. Edward, Orientational distribution of parent-daughter structure of isotactic polypropylene: a study using simultaneous synchrotron WAXS and SAXS, J. Mat. Sci. 43 (2008) 6459—6467.

[23] Z.G. Zhao, Q. Yang, M.Q. Kong, D.H. Tang, Q.Y. Chen, Y. Liu, F.L. Lou, Y.J. Huang, X. Liao, Unusual hierarchical structures of micro-injection molded isotactic polypropylene in presence of an in situ microfibrillar network and a β-nucleating agent, RSC Adv. 5 (2015) 43571—43580.

[24] Z.W. Cai, Y. Zhang, J.Q. Li, F.F. Xue, Y.R. Shang, X.H. He, J.C. Feng, Z.H. Wu, S.C. Jiang, Real time synchrotron SAXS and WAXS investigations on temper-ature related deformation and transitions of β-iPP with uniaxial stretching, Polymer 53 (2012) 1593—1601.

[25] Y. Zhang, L. Zhang, H. Liu, H.N. Du, J. Zhang, T. Wang, X.W. Zhang, Novel approach to tune mechanics of β-nucleation agent nucleated polypropylene: role of oriented β spherulite, Polymer 54 (2013) 6026—6035.

[26] X.H. Liu, K. Dai, X.Q. Hao, G.Q. Zheng, C.T. Liu, D.W. Schubert, C.Y. Shen, Crystalline structure of injection molded β-isotactic Polypropylene: analysis of the oriented shear zone, Ind. Eng. Chem. Res. 52 (2013) 11996—12002.

[27] X.H. Liu, Y.M. Pan, G.Q. Zheng, C.T. Liu, Suppression of the hierarchical structure of water-assisted injection moulded iPP in the presence of a β-nucleating agent and lamellar branching of a β-crystal, RSC Adv. 6 (2016) 68969—68972.

[28] J. Lipp, M. Shuster, G. Feldman, Y. Cohen, Oriented crystallization in poly-propylene fibers induced by a sorbitol-based nucleator, Macromolecules 41 (2008) 136—140.

[29] M. Fujiyama, T. Wakino, Y. Kawasaki, Structure of skin layer in injection-molded polypropylene, J. Appl. Polym. Sci. 35 (1988) 29—49.

[30] Y. Wang, J.L. Pan, Y. Mao, Z.M. Li, L. Li, B.S. Hsiao, Spatial distribution of γ-crystals in metallocene-made isotactic polypropylene crystallized under combined thermal and flow fields, J. Phys. Chem. B 114 (2010) 6806—6816.

[31] C.Y. Zhang, B. Wang, J.H. Yang, D. Ding, X.R. Yan, G.Q. Zheng, K. Dai, C.T. Liu, Z.H. Guo, Synergies among the self-assembled β-nucleating agent and the sheared isotactic polypropylene matrix, Polymer 60 (2015) 40—49.

[32] M. Yamaguchi, T. Fukui, K. Okamoto, S. Sasaki, Y. Uchiyama, C. Ueoka, Anomalous molecular orientation of isotactic polypropylene sheet containing N,N-dicyclohexyl-2, 6-naphthalenedicarboxamide, Polymer 50 (2009) 1497—1504.

[33] M. Fujiyama, Structures and properties of injection moldings of β-crystal nucleator-added polypropylenes: Part 1 effect of β-crystal nucleator content, Int. Polym. Proc. 10 (1995) 172—178.

[34] Z.Z. Liu, G.Q. Zheng, H.L. Zheng, K. Dai, C.T. Liu, J.B. Chen, C.Y. Shen, Micro-structure and mechanical properties of isotactic polypropylene films fabri-cated via melt-extrusion and uniaxial-stretching, J. Macrom. Sci. Part B 55 (2015) 158—174.

[35] B. Larin, C.A. Avila-Orta, R.H. Somani, B.S. Hsiao, G. Marom, Combined effect of shear and fibrous fillers on orientation-induced crystallization in disconti-uous aramid fiber/isotactic polypropylene composites, Polymer 49 (2008) 295—302.

[36] K. Cho, D.N. Saheb, H. Yang, B.-I. Kang, J. Kim, S.-S. Lee, Memory effect of locally ordered α-phase in the melting and phase transformation behavior of β-isotactic polypropylene, Polymer 44 (2003) 4053—4059.

[37] J.X. Li, W.L. Cheung, D. Jia, A study on the heat of fusion of β-polypropylene, Polymer 40 (1999) 1219—1222.

[38] Q. Yuan, W. Jiang, L. An, Study of β—α recrystallization of the polypropylene, Colloid. Polym. Sci. 282 (2004) 1236—1241.

[39] D.S. Homminga, B. Goderis, V.B.F. Mathot, G. Groeninckx, Crystallization behavior of polymer/montmorillonite nanocomposites. Part III. Polyamide-6/montmorillonite nanocomposites, influence of matrix molecular weight, and of montmorillonite type and concentration, Polymer 47 (2006) 1630—1639.

[40] M. Jin, K.J. Liu, H. Liu, Y. Zhang, H.N. Du, X.P. Li, J. Zhang, Effects of polyolefin elastomer and β-nucleating agent on morphological evolution of isotactic polypropylene under an intensive shear rate, Polym. Test. 39 (2014) 1—11.

[41] M.A. Sabino, G. Ronca, A.J. Müller, Heterogeneous nucleation and self-nucleation of poly (p-dioxanone), J. Mat. Sci. 35 (2000) 5071—5084.

[42] J.D. Hoffman, Role of reptation in the rate of crystallization of polyethylene fractions from the melt, Polymer 23 (1982) 656—670.

[43] D. Roylance, Stress-strain Curves, Massachusetts Institute of Technology study, Cambridge, 2001.

[44] Y.F. Men, J. Rieger, G. Strobl, Role of the entangled amorphous network in tensile deformation of semicrystalline polymers, Phys. Rev. Lett. 91 (2003) 095502.

[45] Y. Lu, W. Yang, K. Zhang, M.B. Yang, Stress relaxation behavior of high density polyethylene (HDPE) articles molded by gas-assisted injection molding, Polym. Test. 29 (2010) 866—871.

[46] A. Lustiger, R. Markham, Importance of tie molecules in preventing poly-ethylene fracture under long-term loading conditions, Polymer 24 (1983) 1647—1654.

[47] C.S. Jao, Y. Wang, C. Wang, Novel elastic nanofibers of syndiotactic poly-propylene obtained from electrospinning, Eur. Polym. J. 54 (2014) 181—189.

[48] B. Na, Q. Zhang, H. Yang, Q. Fu, Y.F. Men, High viscous stress of oriented polyolefins under uniaxial tensile deformation, Chin. J. Polym. Sci. 25 (2007) 285—290.

[49] Y. Gao, K. Ren, N.Y. Ning, Q. Fu, K. Wang, Q. Zhang, Stretching-induced interfacial crystalline structures and relevant mechanical properties in melt-spun polypropylene/whisker composite fibers, Polymer 53 (2012) 2792—2801.